



## Comparison of Conventional and Modified Burners in Performance with Different Fuels using a Linear and a Non-linear Eddy-viscosity Turbulence Model

M. U. Yangaz†, G. A. Çiftçiöğlü and M. A. N. Kadirgan

*Department of Mechanical Engineering, Faculty of Engineering, Marmara University, Istanbul, 34722, Turkey*

†Corresponding Author Email: [murat.yangaz@marmara.edu.tr](mailto:murat.yangaz@marmara.edu.tr)

(Received November 25, 2018; accepted February 17, 2019)

### ABSTRACT

Energy sources must be used efficiently to provide the sufficient amount of energy for the still-growing population in the world, already threatened by the effects of global warming. The significant increase in the use of natural resources causes serious problems due to its unsustainable situation. Therefore, exhaust gases/emissions must be reduced to prevent more damage on the environment. This study aims to provide solutions for a sustainable ecosystem by lowering emissions such as CO, unburnt HC, NO<sub>x</sub>, and enhancing the combustion efficiency in a certain type/scale industrial burner. In that way, some geometric modifications (on furnace design and the connected burner) have been applied on the conventional type burners to benefit the effects of preheating of combustion air. Modified geometries have been analyzed numerically and compared with the conventional design's results. Moreover, the comparison between a linear and non-linear turbulence model has been given in terms of simulation results. Major findings indicate that Burner-1 has significantly lower emissions compared to the others. Preheating effect coupled with the flue gas recirculation (FGR) seems to work well in terms of performance and emissions. Also, a significant difference between linear and non-linear turbulence model appeared on the emission characteristics for the same simulations.

**Keywords:** Computational fluid dynamics; Combustion; Preheating; Emissions; Flue gas recirculation.

### NOMENCLATURE

$A_0$	constant	$IFGR$	external flue gas recirculation
$a_1$	constant	$k$	turbulent kinetic energy
$A_s$	constant	$T$	temperature
$BG$	biogas	$u$	flow velocity
$C_1$	constant	$V_k$	diffusion velocity of kth specie
$C_2$	constant	$Y_k$	mass fraction
$C_{1\epsilon}$	constant	$Y_M$	fluctuating dilatation term
$C_{3\epsilon}$	constant	$\alpha$	scattering coefficient
$CAD$	computer aided design	$\mathcal{E}$	turbulent dissipation rate
$CRN$	chemical reactive network	$\epsilon_{ij}$	dynamic viscosity
$C_{ij}$	convection term	$\mu$	dynamic viscosity
$C_\mu$	constant	$LHS$	left hand side
$CFD$	computational fluid dynamics	$LPG$	liquefied petroleum gas
$D_{T,ij}$	turbulent diffusion term	$LTD$	local time derivative
$D_{L,ij}$	molecular diffusion term	$n$	refractive index
$e$	internal energy	$NG$	natural gas
$EFGR$	external flue gas recirculation	$p$	pressure
$ER$	equivalence ratio	$P_{ij}$	production of stress
$F$	force	$P_k$	production of turbulent kinetic energy
$FGR$	flue gas recirculation	$P_b$	prod. of turb. kin. en. due to buoyancy
$g$	gravitational acceleration	$S$	source term
$GMS$	gas mixing system	$S_e$	source term
$I$	spectral intensity	$S_\epsilon$	source term

$S_{ij}$	strain tensor	$TKE$	turbulent kinetic energy
$S_M$	source term	$\mu_t$	turbulent (eddy) viscosity
$S_{rad}$	source term	$\rho$	density
$PDF$	probability density function	$\sigma_\epsilon$	constant
$\vec{r}$	position vector	$\sigma_k$	constant
$RHS$	right hand side	$\sigma_s$	absorption coefficient
$RSM$	reynolds stress model	$\tau$	stress tensor
$RTE$	radiative transfer function	$\Phi$	phase function
$\vec{s}$	direction vector	$\varphi_{ij}$	production of strain
$\vec{s}'$	scattering direction vector	$\Omega'$	solid angle
$SRF$	solid recovered fuel		
$TDR$	turbulent dissipation rate		

## 1. INTRODUCTION

Efficient energy use is a necessity due to the increase in population of the world and the energy demand that it creates. In addition, depleting fossil fuels and the emission issues lead to many studies and applications on the subject, since it is affecting the environment. On the other hand, there are efforts to increase the share of the renewable and less emissive resources such as biofuels and hydrogen in energy generation processes. It is important to promote clean energy sources or use the conventional sources in an efficient way in order to maintain economic and environmental sustainability (Albrecht *et al.*, 2017).

Concerns over the global environment have led to strict rules in combustion industry, especially for reducing NO<sub>x</sub> emissions. NO<sub>x</sub> mechanisms occur at higher operating temperature, and lean premixed combustion in this way has many aspects as an approach toward reduced NO<sub>x</sub> emissions. However, there are technical challenges such as the tendency of the dynamic flame to become unstable and lean blow off limit.

This study aims to provide solutions for a sustainable environment by enhancing the thermal efficiency and reducing the hazardous emissions during combustion process in a certain type/scale of industrial burners by applying geometric improvements. Also, comparison of a linear and a non-linear turbulence models has been given in terms of temperature distribution and emission levels.

There are many studies on reaching lower emission values for the burners in the literature. In one of them, researchers developed a new methodology for the design optimization of low emission (CO and NO<sub>x</sub>) burner in a 2 MW superheated steam boiler system (Chacón *et al.*, 2006). Other group of scientists investigated the combustion and NO<sub>x</sub> emissions in two swirl burners, base geometry and its optimized form, and 600 MW wall-fired boiler (Zhou *et al.*, 2014). They showed that NO<sub>x</sub> emission had decreased from 440 to 265 mg/Nm<sup>3</sup> at 6% O<sub>2</sub> in optimized burner. However, unburnt carbon content of the fly ash had increased from 1.02% to 1.33%. In another study, optimization of a gas mixing system (GMS) of premixed burner using CFD techniques was carried out (Zhang *et al.*, 2014). They proved that the uniformity at the outlet of GMS had significant influence on emissions. Improved design resulted in an increase by 234.2% and 2.9% on the

uniformity of velocity and fuel–gas mixing of single ejector, respectively. They stated that above improvements could be useful for premixed burners.

Due to high NO<sub>x</sub> output of hydrogen combustion systems, hydrogen is not a preferred energy source in burners. However, a group of scientists (Cappelletti *et al.*, 2017) published a paper on a gas turbine burner using hydrogen as fuel. Their solution is a lean premixed combustion with use of a new axial swirler and a co-flow injection. The best result they reached was 17 ppm as the lowest value of NO<sub>x</sub> emission.

Oxy-fuel coal combustion was studied in several applications using various methods and models (Gaikwad *et al.*, 2017; Jovanović *et al.*, 2017; Vega *et al.*, 2015). One of the outcomes was that SST k-omega model predicted the results correctly, when compared to the experimental data and Large Eddy Simulation modeling. They also investigated the effect of combustion environments such as oxy-steam (O<sub>2</sub>/H<sub>2</sub>O), air and oxy-RFG (O<sub>2</sub>/CO<sub>2</sub>) on temperature and NO concentration distributions. Results shows that minimum NO<sub>x</sub> formation occurred in oxy-steam environment. Some geometrical parameters such as combustion chamber length and diameter were investigated numerically. The results had shown the minimum length where total combustion of the fuel had been achieved. According to their evaluation, they found optimum values for the parameters, namely the chamber diameter as 1500 mm, chamber length as 6 m, and quarl angle as 50°.

Furthermore, Kuang *et al.* (2014) made a low cost geometrical modifications/improvements on a 300-MW down-fired furnace. They set up a scaled experimental bench to investigate the flow characteristics inside the furnace. By shortening the area of the secondary air port, they prevented a severe asymmetric combustion which causes poor performance.

In another study, new burner concepts were tested for the non-catalytic partial oxidation of natural gas in a numerical study (Förster *et al.*, 2017). They used a detailed reaction mechanism containing 28 species and 112 reactions. The new models had proved that the optimized concepts had significant higher conversion rate, which could create a possibility for more compact reactor design or, alternatively, for a higher output. They also validated the final designs

experimentally. Moreover, measurements were in good agreement with CFD results. In a recent research (Chen *et al.*, 2017) was conducted on a low NO<sub>x</sub> technique of folded flame pattern based on fuel staging burner, which used natural gas as fuel. They studied on two type of burners. Modifications that they offered were validated by their simulations to achieve the folded flame pattern. They also stated that it could affect the reactions and reduce hot spots in temperature field, thus results in a considerable NO reduction. Furthermore, they suggested that different flame patterns could be studied in order to examine the folded flame pattern. On the other hand, the optimization of geometrical parameters was carried out on a fuel-staged low NO<sub>x</sub> gas burner in another similar study (Liu *et al.*, 2017). They investigated the effect of position of the staged gun, the primary gas and the staged gas injection angles on the flame size and NO emission. They validated the results with the measurements of the flue gas samples such as O<sub>2</sub> and NO concentrations. They found that the staged gun was the most effective on NO emission, followed by the staged gas injection and primary gas injection angles respectively. At the end, they proposed a single value for each of the parameters they changed.

Moreover, a biogas combustion process in a 10kW-burner was observed in a numerical study. They investigated the combustion characteristics, effect of preheating, influence of H<sub>2</sub>S amount on SO<sub>2</sub> emissions. They carried out CFD simulations on different gas compositions. According to the results, they stated that preheating process caused flame temperature to rise (Ilbaş *et al.*, 2016). In addition, Zhen *et al.* (2016) performed an experimental study about the preheating and dilution effects to analyze the change in thermal performance and emission characteristics in a domestic cooker burner using the FGR concept. They observed higher burning velocities and an increase in CO and NO<sub>x</sub> emissions with preheating. However, they stated that its combined effects with dilution had provided feasible outcomes in domestic burners. Harish *et al.* (2018) conducted an experimental study to investigate the flame characteristics and stability in a non-premixed biogas combustion. They changed the volumetric flow rates of biogas and velocity of air. In result, they compared the flame stabilities with pure methane cases. In a recent study, Tu *et al.* (2018) implemented FGR technique for reducing NO<sub>x</sub> emissions in a biomass fired boiler system. They aimed to observe the NO<sub>x</sub> emission mechanisms and the limits of internal FGR (IFGR) method on combustion characteristics and emissions. They found that IFGR was causing the peak temperatures inside to drop and depending on this outcome, thermal, N<sub>2</sub>O and NNH pathways of NO<sub>x</sub> formation had also been reduced.

Mohammed *et al.* (2018) carried out numerical simulations on the tip-opening mechanism in a premixed combustion of propane-air mixture. They investigated the temperature distribution, reaction rates and net production rate for fuel-rich mixtures under different conditions of equivalence ratios (ER). They observed that the tip-opening concept beginning from 1.4 of ER. The results had showed

that tip-opening had been found to be increasing as the mixture became richer. They also stated that volumetrically the rate of heat release was below 50% of the rate of heat release at flame shoulders and the thickness of the flame tip was found to be closer to 30% between 1.3 and 1.4 of ER.

The extinction limits were investigated for rich and lean fuel flames in a non-premixed coaxial burner with swirl effects. The experiments were made using methane and two different blends of CH<sub>4</sub>/C<sub>x</sub>H<sub>y</sub>/N<sub>2</sub>. The observations were done by considering the equivalence ratios. The achievements had proven that stream of methane was enhancing the blowout limits where other fuels show no similar trends. A parallel increase in C<sub>x</sub>H<sub>y</sub> and N<sub>2</sub> had suggested a deterioration in extinction limits for lean fuel and improvement for rich fuel flames (Jerzak, 2018).

Different articles about various emission reduction techniques exist in the literature. One of them is on the flameless combustion method, which was proposed as a viable solution to the emission problem at hand. Mentioned study provided information about the flow field and the emissions inside the combustor using CFD and chemical reactor network (CRN) respectively. CRN had shown the dominant pathway for NO<sub>x</sub> formation was the prompt NO<sub>x</sub> mechanism. In addition, they made some suggestions for improving the design by modifying the mixing ratios (Perpignan *et al.*, 2018).

Production costs are another factor for trying to find better options with considering the efficiency and emissions aspects. The cement industry, as a paper mentions about it (Pedersen *et al.*, 2017), aims to come up with combustion systems working with alternative fuels to reduce their CO<sub>2</sub> and the costs. They discovered the delay that co-firing with solid recovered fuel (SRF) by around 2 m and when compared to a fossil fuel flame, low intensity and flame temperatures had been observed. They explained this phenomenon by the larger particle sizes and the moisture content of alternative fuels. The results they saw was on the quality of the cement. Their modification on the burner had improved the dispersion of the fuel and provided early ignition, which produce an enhancement in cement quality.

The effect of swirl number and composition of oxidizers was investigated for non-premixed methane flames numerically (Rashwan, 2018). They carried out CFD simulations with using 30, 40 and 50% of oxygen fractions for evaluating the flexibility of the oxidizer on combustion characteristics. The results had revealed that the thermal NO<sub>x</sub> mechanism could be reduced with the increase in swirl number by 95%. Ouali *et al.* (2016) also studied the variation of swirl number (0.5 to 1.0) and equivalence ratio (0.6 to 1.4). with k-ε and LES models resulting in similar outputs.

## 2. MATERIAL AND METHODS

This section provides a detailed information on the mathematical models used in the study, how the simulation process was handled and which

parameters were used. The values and the governing equations also have been presented and explained extensively.

### 2.1 Methodology

In this study, existing geometries of different combustors have been evaluated and prepared for the solution. The variables of the system mainly consist of fuel composition, preheating and as well as geometric alterations which enhances emission reduction on the solid body. After that, to perform a parametric study, these parameters have been changed, then the results have been evaluated. Evaluated data gave information about the operating conditions of the system with the given boundary conditions. Finally, all the information has been used to define the desired and optimum operating zones. All these processes have been done by using a commercial software ANSYS Products including Fluent 17.2.

### 2.2 Methods for Reducing NO<sub>x</sub> Emissions

As it was mentioned before, NO<sub>x</sub> emissions can be reduced by using various techniques, consisting of common and rather new ones such as the concepts of staged combustion, flue gas recirculation (FGR), premixed combustion and oxy-fuel combustion (Colannino, 2006; Jr, 2013; Turns, 2012). In this study, the effects of internal FGR is examined thoroughly.

FGR is a very effective way to ensure reduced NO<sub>x</sub> emissions as well as to achieve combustion that is more efficient. There are two types of FGR; internal flue gas recirculation (IFGR) and external flue gas recirculation (EFGR).

### 2.3 Governing Equations

Governing equations used in the simulations are given below (Kakaç *et al.*, 2007; Turns, 2012):

Mass Conservation Equation:

$$\frac{\partial \rho}{\partial t} + \nabla \cdot (\rho \vec{u}) = S_M \quad (1)$$

Conservation of mass corresponds to the summation of the change in density over time and the net mass flow across the boundaries of the control volume by convection.

Momentum Conservation Equation:

$$\frac{\partial}{\partial t} (\rho \vec{u}) + \nabla \cdot (\rho \vec{u} \vec{u}) = -\nabla p + \nabla \cdot (\vec{\tau}) + \rho \vec{g} + \vec{F} \quad (2)$$

Conservation of momentum can be identified as the summation of the change of velocity with time and convective term on one side, which equals to the summation of pressure gradient, diffusion term, body force term and the other source terms on the other side of the equation.

Energy Equation:

$$\frac{\partial}{\partial t} (\rho \epsilon) - \nabla \cdot (\rho \epsilon \vec{u}) = \frac{\partial p}{\partial t} + \nabla \cdot (k \nabla T) + S_t \quad (3)$$

Energy equation represents the summation of local

change in the internal energy with time and convection term on the left hand side (LHS) of the equation. They equal to the summation of pressure work, diffusion (heat flux) term and irreversible mechanical energy transfer into heat on the right hand side (RHS).

Simulations have been carried out using both linear and non-linear eddy viscosity models. Realizable k-ε turbulence model has been utilized as the linear and Reynolds Stress turbulence model has been used as the non-linear eddy viscosity model.

Realizable k-ε turbulence model, and transport equation for the model are given below:

k equation:

$$\frac{\partial}{\partial t} (\rho k) + \frac{\partial}{\partial x_i} (\rho k u_i) = \frac{\partial}{\partial x_j} \left( \left( \mu + \frac{\mu_t}{\sigma_\epsilon} \right) \frac{\partial k}{\partial x_j} \right) + P_k - P_b - \rho \epsilon - Y_M + S_k \quad (4)$$

ε equation:

$$\frac{\partial}{\partial t} (\rho \epsilon) + \frac{\partial}{\partial x_i} (\rho \epsilon u_i) = \frac{\partial}{\partial x_j} \left( \left( \mu + \frac{\mu_t}{\sigma_\epsilon} \right) \frac{\partial \epsilon}{\partial x_j} \right) + \rho C_1 S_\epsilon - \rho C_2 \frac{\epsilon^2}{k + \sqrt{g \epsilon}} + C_{1\epsilon} \frac{\epsilon}{k} C_{3\epsilon} P_b + S_\epsilon \quad (5)$$

$$C_1 = \max \left[ 0.43, \frac{\eta}{\eta + 5} \right] \quad (6)$$

$$\eta = S \frac{k}{\epsilon} \quad (7)$$

$$S = \sqrt{2 S_{ij} S_{ij}} \quad (8)$$

in Realizable k-ε turbulence model, turbulent (eddy) viscosity can be calculated using the below formula:

$$\mu_t = \rho C_\mu \frac{k^2}{\epsilon} \quad (9)$$

In Eq. (4), the first term on the left hand side (LHS) can be described as the rate of the change in turbulent kinetic energy (TKE), second term on the LHS can be defined as the transport of TKE by convection. The first term on the right hand side (RHS) represents the transport of TKE by diffusion,  $P_k$  demonstrates the production of TKE.  $P_b$  symbolizes the production of TKE due to buoyancy, fourth term on the RHS represents the destruction of TKE,  $Y_M$  demonstrates the fluctuating dilatation term. Finally, the last term,  $S_k$  is defined as a source term.

Equation (5) can be expressed as the rate of change of turbulent dissipation rate (TDR) summation with transport of TDR by convection, which equals to the transport of TDR by diffusion and production of TDR difference by the destruction of TDR.

Due to the realizability of the model, it satisfies the

mathematical constraints on Reynolds stresses thoroughly and thus it ensures consistency with turbulent flow physics. It can also predict the spreading rate for plane and round jets accurately. It has been tested extensively over many types of flows including boundary layer and channel flows, and jets and free flows (Shih *et al.*, 1995).

Table 1 shows the model constants of k-ε turbulence model.

**Table 1 k-ε turbulence model constants**

C <sub>1ε</sub>	C <sub>2</sub>	σ <sub>k</sub>	σ <sub>ε</sub>	A <sub>0</sub>	A <sub>s</sub>
1.44	1.9	1.0	1.2	4.04	cosφ

Reynolds Stress turbulence model and its transport equation is given below (Craft *et al.*, 1996; Hanjalić *et al.*, 2011; Launder *et al.*, 1975):

$$\begin{aligned} \frac{\partial}{\partial t}(\rho \overline{u_i u_j}) + \frac{\partial}{\partial x_k}(\rho u_k \overline{u_i u_j}) = & \\ - \frac{\partial}{\partial x_k} \left[ \rho \overline{u_i u_j u_k} + p(\delta_{kj} \overline{u_i} + \delta_{ik} \overline{u_j}) \right] & \\ + \frac{\partial}{\partial x_k} \left[ \mu \frac{\partial}{\partial x_k} (\overline{u_i u_j}) \right] & \\ - \rho \left( \overline{u_i u_k} \frac{\partial u_j}{\partial x_k} + \overline{u_j u_k} \frac{\partial u_i}{\partial x_k} \right) + p \left( \frac{\partial u_i}{\partial x_j} + \frac{\partial u_j}{\partial x_i} \right) & \\ - 2\mu \frac{\partial u_i}{\partial x_k} \frac{\partial u_j}{\partial x_k} - 2\rho \Omega_k \left( \overline{u_j u_m} \varepsilon_{ikm} + \overline{u_i u_m} \varepsilon_{jkm} \right) & \end{aligned} \quad (10)$$

or in a simplified and more explanatory way:

$$\begin{aligned} LTD + C_{ij} = D_{T,ij} + D_{L,ij} & \\ + P_{ij} + \varphi_{ij} - \epsilon_{ij} + F_{ij} & \end{aligned} \quad (11)$$

Where LTD is the local time derivative, C<sub>ij</sub> symbolize the convection term, D<sub>T,ij</sub> is the turbulent diffusion term, D<sub>L,ij</sub> equals the molecular diffusion, P<sub>ij</sub> stands for production of stress, φ<sub>ij</sub> is the term for pressure strain, ε<sub>ij</sub> is for the dissipation term and F<sub>ij</sub> stands for production by system rotation. Among the terms above, only D<sub>T,ij</sub>, φ<sub>ij</sub>, ε<sub>ij</sub> must be modelled for the closure of equation system. Because of the significant drawbacks of linear eddy viscosity models (i.e. k-ε, k-ω etc.) in modelling flows with high anisotropy, variations in pressure fields, acceleration and decelerations, a non-linear eddy viscosity turbulence model, RSM has been preferred.

The mass fractions of multiple species in a reacting flow can be obtained by the use of the continuity equation for species given below:

Momentum Conservation Equation:

$$\frac{\partial \rho Y_k}{\partial t} + \nabla Y_k * (\rho \vec{v}) = \nabla * (-\rho V_k Y_k) + \omega_k \quad (12)$$

In the equation above, ρ is density,  $\vec{v}$  is the velocity vector, V<sub>k</sub> is the diffusion velocity of kth specie. The term ω<sub>k</sub>, symbolizes the production rate of k<sup>th</sup> specie. ρV<sub>k</sub>Y<sub>k</sub>, represents the diffusive mass flux.

In this study, Discrete Ordinates (DO) model has been chosen for its capability of considering the entire range of optical thickness, and its applicability in coupled solutions. Radiative Transfer Equation (RTE) of the model is given below:

$$\begin{aligned} \nabla \cdot (I(\vec{r}, \vec{s}) \vec{s}) + (\alpha + \sigma_s) I(\vec{r}, \vec{s}) & \\ = \alpha n^2 \frac{\sigma T^4}{\pi} + \frac{\sigma_s}{4\pi} \int_0^{4\pi} I(\vec{r}, \vec{s}') \varphi(\vec{s}, \vec{s}') d\Omega' & \end{aligned} \quad (13)$$

where I is the spectral intensity,  $\vec{r}$ ,  $\vec{s}$  and  $\vec{s}'$  are the position, direction and scattering direction vectors respectively, n is the refractive index, α and σ<sub>s</sub> represent the scattering and absorption coefficients. Φ is the phase function. Ω' remarks the solid angle.

Non-premixed model works on the approach called Probability Density Function (PDF). PDF techniques are an effective way for the solution of the interaction between turbulence and chemistry. It includes the effects of fluctuations in turbulence and chemical composition for flows that contains reactions and turbulence together. It calculates the concentration of species using the predicted mixture fractions. PDF method depends on the solution of a modeled transport equation for a specific location and time which explains its thermochemical state of a reactive domain (ANSYS, 2017; Frouzakis, 2011; Haworth, 2010; Tannehill *et al.*, 2013).

### 3. ANALYSIS OF 1.3-MW INDUSTRIAL BURNER

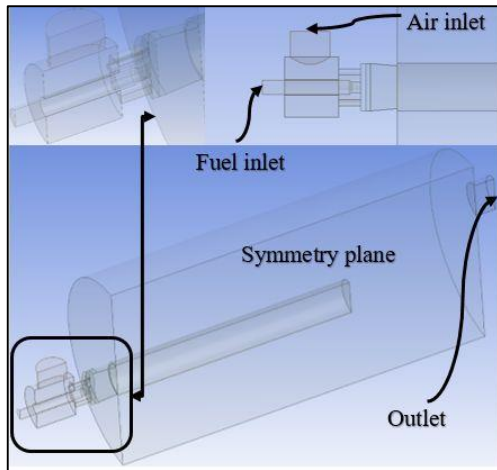
In this section, applications of preheating effects have been discussed in detail for a 1.3-MW burner. Four different design cases including the conventional one have been used. These are:

- 1.3-MW Conventional Burner (no modifications added)
- Burner#1: A dominant IFGR modification is added using tubular air flow.
- Burner#2: A dominant preheating modification is built in.
- Burner#3: Heat transfer ability by preheating modification is increased.

#### 3.1 Flow Domains & Grids

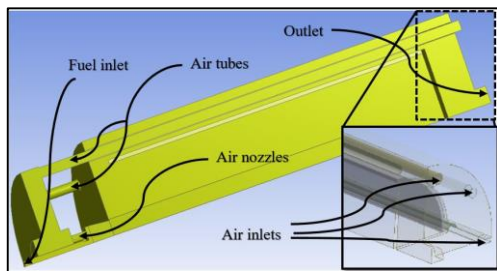
Fig. 1 demonstrates general forms of CAD domain with given boundaries and close look-ups. The geometry of the base case consists of only one air-inlet (d=368 mm), a fuel inlet (d=133.7 mm), eight main air-nozzles (d=60 mm), eight smaller air-nozzles (d=25 mm) between the main ones. The geometry is symmetrical, so half of the geometry was used in the simulations to reduce the cell count, thus

resulting a decrease in the simulation time.



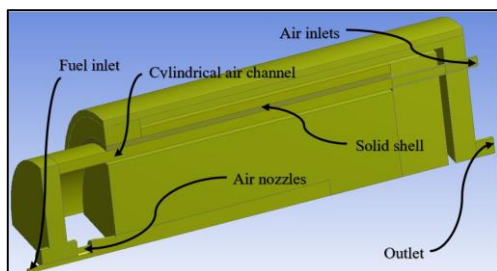
**Fig. 1. CAD model of the conventional burner.**

Fig. 2 illustrates the geometry of a burner and the furnace with capabilities of both internal flue gas recirculation and preheating of combustion air.



**Fig. 2. Burner #1 and furnace design concept.**

The air is coming from the tubes at the end of the furnace, passing over the surface of the furnace and inside the flue gas channel. The air gets heated in the process and thus reducing the temperatures of both the flue gas and the furnace body. The material of air tubes was defined as cast iron with a thermal conductivity of 80 W/m-K. Fig. 3 demonstrates the geometry of a burner and the furnace with capability of preheating the combustion air. In this design, instead of using tube type air channels, a cylindrical structure has been attached to the outer surface of the furnace.



**Fig. 3. Burner #2 and furnace design concept.**

Figure 4 shows the geometry of a burner and the furnace with capability of preheating the combustion air with an increase in heat transfer area between flue gas channel and the combustion air channel.

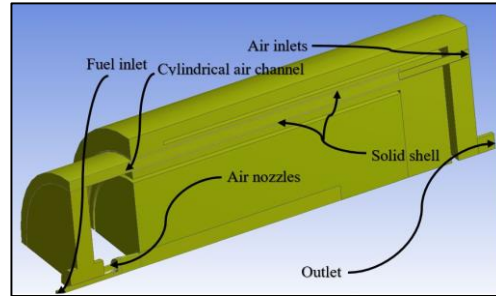


**Fig. 4. Burner #3 and furnace design concept.**

Polyhedral and hexahedral mesh structure was used throughout the whole pre-processing stage for each design.

Due to the complexity of the system to be simulated, mesh generation process was immensely critical. Therefore, smaller sized cells have been created around the region where the flame would form. Cell sizes in the other important regions have also been defined accordingly in order not to affect the solutions badly in terms of consistency, accuracy, stability and other computational entities.

For the conventional case, the chosen cell count was 3518495. The cell counts of Burner #1, #2 and #3 are 1514458, 1600595 and 2315818 respectively. In addition, the geometry for each design has been divided into many bodies to handle the mesh structure better in both quality and achieving lower cell count. Three different grid densities have been tried for each design with biogas as the fuel. Results have been given in Fig. 5. According to the small differences which have been evaluated for two selected parameters, it can be said that mesh independency has been achieved.

### 3.2 Simulation Parameters

Simulations have been carried out with four different gases: hydrogen (100% mol. H<sub>2</sub>), since natural gas mainly consists of methane, instead of including full list of species, only methane (100% mol. CH<sub>4</sub>) has been used in the simulations. LPG (20% C<sub>3</sub>H<sub>8</sub>, 80% C<sub>4</sub>H<sub>10</sub>), and biogas (65% CH<sub>4</sub>, 35% CO<sub>2</sub>) are the other gases that have been chosen for the calculations. The other parameter is the geometric alterations on the designs of the base model, which have been changed in order to lower emissions and improve efficiency.

Details of simulation parameters including the information about the boundary conditions have been given in Table 2.

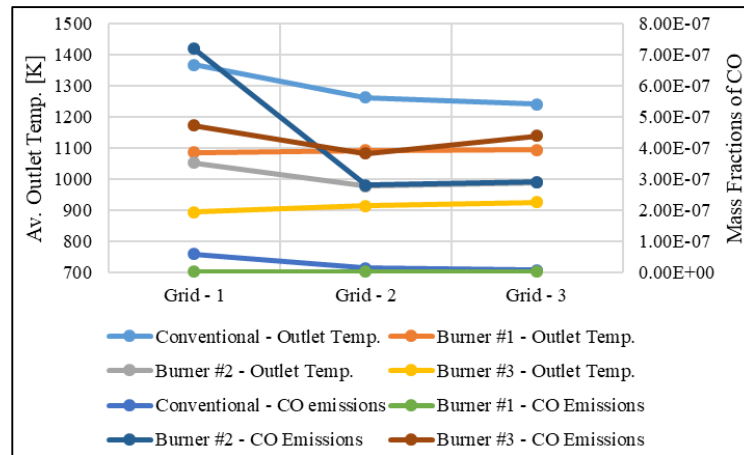


Fig. 5. Results of the mesh independency study.

Table 2 Simulation Parameters

Atmospheric Pressure	101,325 Pa
Fuel Inlet (mass-flow-inlet)	0.027901 (CH <sub>4</sub> ), 0.029211 (LPG), 0.011062 (H <sub>2</sub> ), 0.066371 (Biogas) kg/s
Air Inlet (mass-flow-inlet)	0.526657 (CH <sub>4</sub> ), 0.495455 (LPG), 0.41763 (H <sub>2</sub> ), 1.252817 (Biogas) kg/s
Fuel Inlet Temperature	300 K
Furnace Wall Temperature	1,273 K
Excess Air Ratio	10%

k-ε model has been chosen as a linear eddy viscosity model to be compared to a non-linear eddy viscosity model, namely RSM.

#### 4. RESULTS AND DISCUSSION

##### 4.1 Results Using a Linear Eddy Viscosity Model

Fig. 6 shows that a significant temperature drop in the outlet region due to the heat transfer of the flue gas to the incoming combustion air except for the conventional burner.

As it can be seen from the temperature distribution along central section, conventional design shows considerable instabilities. It is obvious that a large portion of the unburnt mixture has been emitted from the outlet boundary. On the other hand, the other three concept burners show good qualities both in waste energy saving and homogeneous thermal distribution inside the furnace since it is a desired entity for some industrial application such as metal forming. Preheating effect can easily be noticed by the temperatures, where the combustion air gets

heated just before entering the burner. This application has provided at least 400 K preheating.

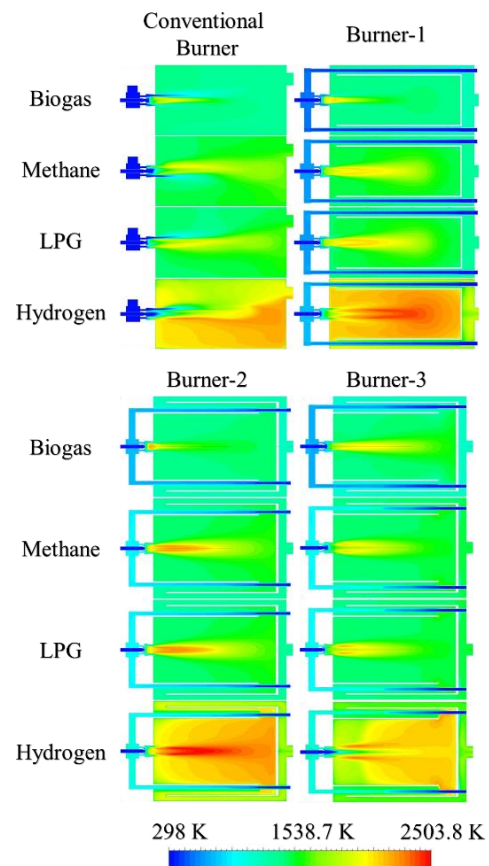
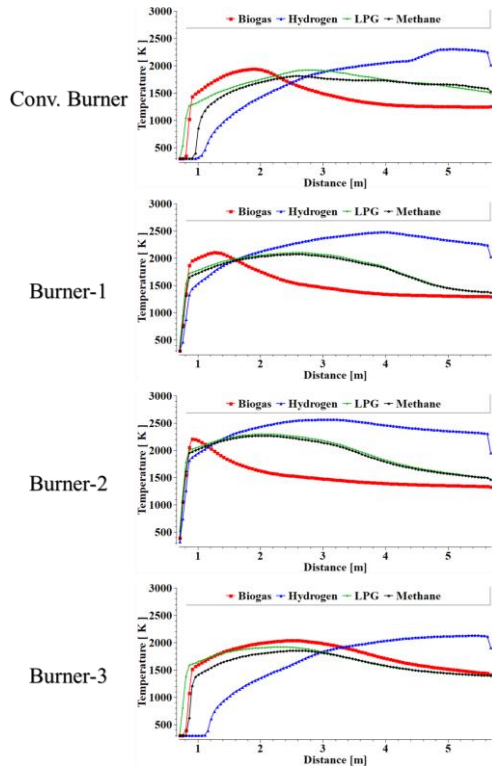


Fig. 6. Temperature distribution in the conventional and Burners 1, 2 & 3.

As it was expected, hydrogen has the maximum flame temperature among the other fuels used in the simulations. Energy output of hydrogen is larger than the others therefore, the flame core reaches higher temperatures. Also, flame lengths are also higher than the others because of high burning velocities compared to other gas fuels. These entities can be

also verified by the axial temperature profiles along the centerline given in Fig. 7. According to the figure, it can be said that Burner – 1 and Burner – 2 have very similar trends in terms of temperature for all types of gases.



**Fig. 7. Axial temperature profiles along the centerline of the burners.**

On the other hand, the highest flame temperatures appear to be inside the Burner – 2 furnace, which may be explained by the positive effects of preheating more than Burner – 1.

Although, Burner – 3 has more heat transfer surfaces inside the flue gas channel, higher speeds inside more contracted channels lead to an increase in convective heat transfer. Moreover, Burner – 3 produces high unburnt hydrogen emission through the outlet boundary in the case of hydrogen combustion. These two factors are the main reasons of lower temperature levels inside the furnace compared to Burner – 2.

Furthermore, the results of the hydrogen cases reveal that Burner-3 and Con. Burner designs show quite similar characteristics in temperature profiles. Lower temperatures can be observed closer to the burner head where the oxidizer and the fuel start to mix.

Burner – 1 here, is benefitting from both preheating and a dominant IFGR concept which results in the best outcome in the current study. Burner – 2 and Burner – 3 have been designed for enhancing the preheating effect which may not be necessary for hydrogen since it raises the flame core temperatures which causes NO formation due to thermal NO pathway. When average thermal NO rates over the

centerline of Con. Burner ( $1e-5$  kmol/m<sup>3</sup>-s) are compared to Burner – 2 ( $2.93e-4$  kmol/m<sup>3</sup>-s), the prediction made above can be easily verified. Lower temperatures of Burner – 3 cause a drop in central NO rates, but at the outlet it is vice versa ( $2.16e-5$  kmol/m<sup>3</sup>-s). This negative effect though can be eliminated via designs that consist and benefit all the techniques mentioned above in the manuscript and the ones that have not been (i.e. design that can manipulate equivalence ratio or the recuperative burner applications).

Although, it may not be as significant and effective as IFGR, the other concepts or designs also have another good quality, which is the increased residence time due to the extended flue gas route to the chimney of the furnace that increases the local pressure losses in momentum equation. To benefit from this, there may be the only way, which is directing the unburnt fuel in a way that it mixes with the spare/unreacted oxidizer inside the chamber or the flue gas channel.

LPG and methane results show similarities according to temperature distribution since their heating values are close to each other. It can be said that the differences are mainly due to the reaction mechanisms.

Figure 8 demonstrates the emission values from the chimney of the furnace. According to the findings below, Burner – 1, which has both preheating and IFGR effect, stands out to be the best concept design in terms of emissions and efficiency. The burner and the furnace design comprised of 8 air entry tubes located at the far end of the furnace, which have considerably lower heat transfer area compared to the other two concept designs.

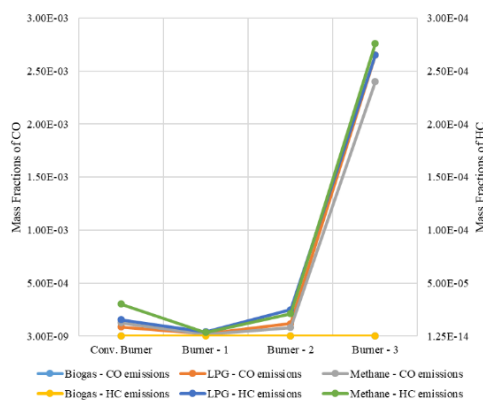


**Fig. 8. Emissions from the outlet in the conventional and Burners 1, 2 & 3.**

CO emission of LPG appears to be slightly higher than the other fuels except for the conventional design. However, the difference in CO emission can easily be seen in RSM simulations. This outcome can be explained by the larger molecules such as butane existence in the fuel. In general, reaction chains of butane are longer in comparison with the other low carbon-numbered HCs, thus requires more energy and residence time to break

the intermolecular bonds in order to form CO as the initial step of HC oxidation after the formation of alkenes and hydrogen molecules at the first stage. The oxidation of CO is rather slow without the involvement of H<sub>2</sub> containing compounds. This is because the step of CO oxidation involving the hydroxyl radical is considerably faster than O and O<sub>2</sub> involving steps.

On the other hand, flue gas motion is different than the others. The mixture comes out of the burner head, enters the furnace, burns out and since the far end is sealed, the mixture, which contains substantial amount of burnt gas together with the remaining unburnt portion, turns back and passes around high temperature area that is close to flame zone. By this way, remaining unreacted mixture also meets up with incoming fresh air and burns before entering the flue gas channel. At the same time, burnt mixture passes close to the flame and reduces flame temperature by the gases inside the flue gas mix that have high specific heat capacity such as H<sub>2</sub>O<sub>(v)</sub>. The general trend in the graph is complying with both the given simulation results as well as the aspects of combustion physics.

The reason behind the low performance of Burner – 3 can be attributed to the higher velocities due to both contracting channels in the flue gas route and the increased heat transfer which raises the internal energy of gas molecules, thereby enhancing their motion towards the exit which is at considerably lower temperature (ambient temperature).

Fig. 9 demonstrates the emission values from the chimney of the furnace.

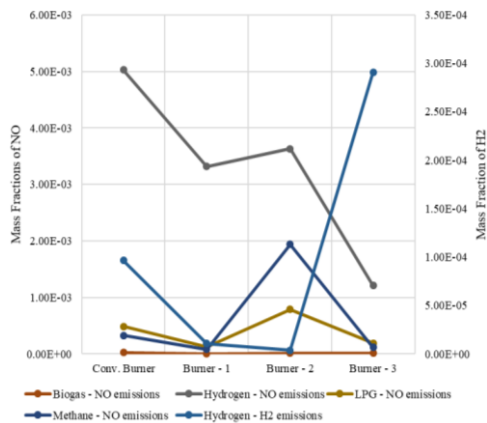


Fig. 9. Mass fractions of NO and unburnt H<sub>2</sub> emissions from the outlet boundary.

Hydrogen cases appear to have the highest amount of NO which is quite understandable. On the other hand, biogas cases have the lowest NO. In between, LPG and methane cases seems to have similar trends. Burner – 3 shows signs of incomplete combustion by looking at the high unburnt H<sub>2</sub> emission for hydrogen case. On the other hand, this may be one of the reasons of low NO emissions and higher velocities also would be effective on this matter.

## 4.2 Results Using a Non-Linear Eddy Viscosity Model

The linear eddy-viscosity-based k-ε models may not be suitable for the considered flow configurations subjected to alternating acceleration and deceleration due to cross-sectional area variation and consequent variations in pressure field. Turbulence-chemistry interaction is another issue which has to be modelled carefully for reacting flows, since it has a significant effect on reactions. Moreover, the linear eddy-viscosity models are insensitive to the sign change of the velocity gradient; the outcome is an always positive production of TKE unless it is manipulated by other means. Therefore, some simulations have been carried out with RSM as the turbulence model to reveal the differences in a clearer manner.

Fig. 10 shows the temperature distributions on the section view at the center of the domain.

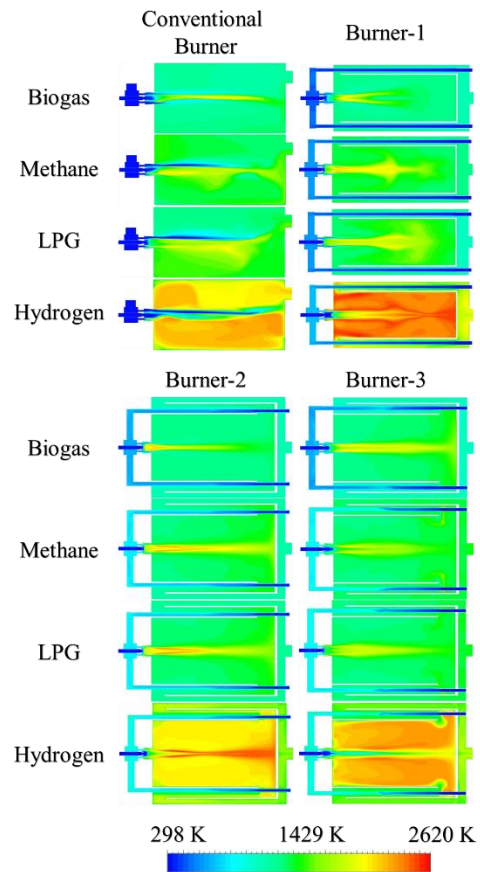


Fig. 10. Temperature distribution in the burners (with RSM turbulence model).

Temperature distribution of the solutions with RSM turbulence model show significant difference on the flame forms. Reduced flame widths and increased flame lengths have been observed in RSM simulations. By looking at the maximum values in the figure above, it can be said that the difference in the temperatures are in 5% range.

Results of RSM turbulence model for the axial temperature profiles along the centerline have been given in Fig. 11. Although, temperature ranges in the

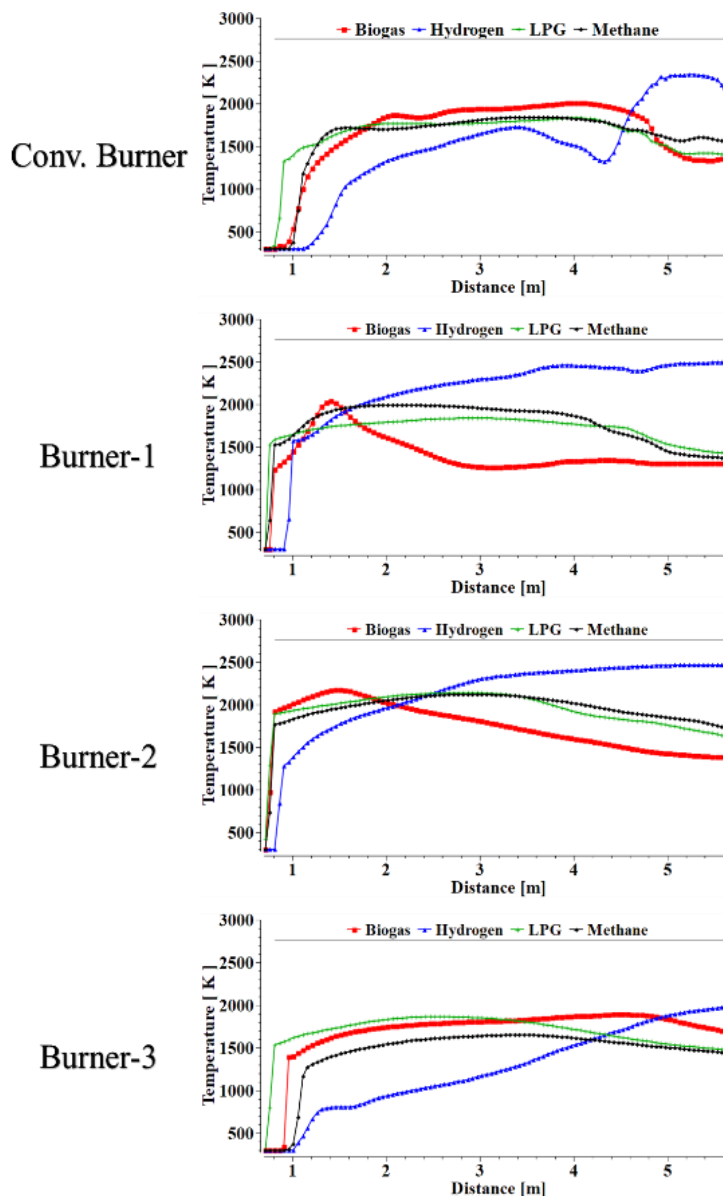


Fig. 11. Axial temperature profiles along the centerline of the burners (with RSM turbulence model).

whole systems differ from the linear eddy viscosity model ( $k-\epsilon$ ), axial temperature values are quite close. Moreover, trends of the curves are very similar except some regions such as the volume around the burner head.

On the other hand, peak temperatures for the Burner – 1 and Burner – 2 are observed further away from the burner head (located between 1.4 and 1.6 m from the fuel and air ports) than  $k-\epsilon$  model predicted except for the hydrogen cases.

Simulation results of hydrogen combustion show that peak temperatures are located closer to the opposite wall in RSM, contrary to  $k-\epsilon$  results in which they are near to the center of the furnace.

Details about the change of emissions with the study parameters have been given in Fig. 11.

RSM turbulence model, which considers the anisotropy in stress tensor, gives slightly different results compared to  $k-\epsilon$  turbulence model results except for the emissions of the conventional burner. RSM model solves 7 additional equations whereas  $k-\epsilon$  model solves 2 additional equations for modelling the turbulence in a flow. According to one’s point of view, it could be a useful option to select a linear eddy viscosity model such as  $k-\epsilon$  for quicker and less computationally expensive simulations. On the other hand, if the accuracy is at the focus, a non-linear eddy viscosity model such as RSM could be utilized in order to achieve more realistic results.

CO emission levels appear to be in the same scale when compared to  $k-\epsilon$  model results. It can be said that the trends are also similar for almost all emissions. However, the difference in the

performance of designs is more distinct with RSM turbulence model which can be the reason of applying a more accurate model on the system.

Fig. 12 illustrates the change in the emission values from the outlet boundary. General trends are compatible with the results of k-ε model. However, H<sub>2</sub> emissions have reached higher levels than in k-ε model results.

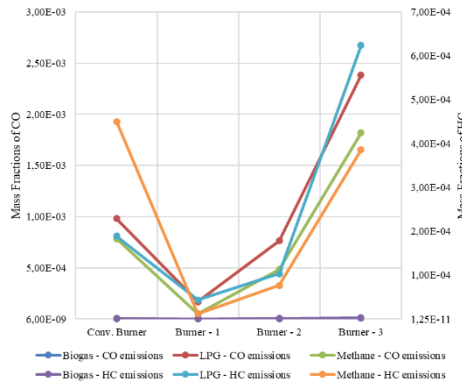


**Fig. 11. CO and HC emissions of the designs (with RSM turbulence model).**

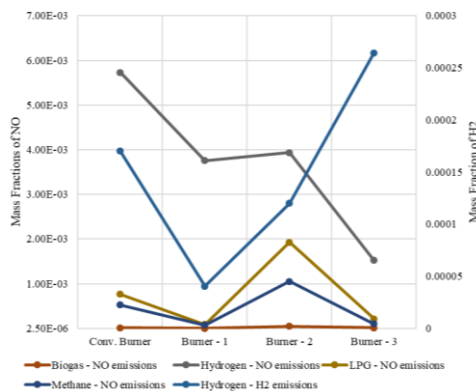


**Fig. 12. NO and H<sub>2</sub> emissions of the designs (with RSM turbulence model).**

It is clear that hydrogen cases have the highest amount of NO again. However, biogas cases results in with the lowest NO levels which can be explained by low energy outputs.

Ratio of useful heat energy (ideal energy output subtracted by heat transfer from the outlet boundary to the environment) to theoretical energy output without considering the heat loss by conduction through the burner and furnace bodies for each case has been given in Table 3.

According to the table above, Burner – 2 appears to have the highest ratios, which can be explained by lower temperature values at the outlet, followed by Burner – 1 and Burner – 3. Conventional burner has the lowest ratios when compared to the other designs.

Although, Burner – 3 has larger heat transfer area over the combustion air channels, the increase in

the velocities inside the flue gas channels due to contractions, leads to higher heat transfer rates enhanced by convection. Therefore, Burner – 3 could not be the best option in terms of this evaluation.

**Table 3 Ratios of useful heat energy to theoretical energy input**

	BG (%)	H <sub>2</sub> (%)	LPG (%)	CH <sub>4</sub> (%)
C. Burner	90.9	82.6	83.4	87.4
Burner - 1	95.1	86.5	89.6	93.7
Burner - 2	92.9	86.3	87.8	89.9
Burner - 3	91.1	84.5	85.0	88.9

Burner – 1 on the other hand, has comparably smaller surfaces for heat transfer on its tubular combustion air channels. Nevertheless, flue gas recirculation helps it to cool off the flame temperatures and by its wider flue gas channels the effects of convection heat transfer plays a lesser role in terms of heat loss from the outlet. Thus, it could be a better selection if it is compared to conventional design and Burner – 3.

## 5. CONCLUSION

Energy efficiency is one of the key elements. Limited resources, growing population and/or advancing technology create a higher energy demand in every branch of life. Renewable and less pollutant technologies became important topics and raised concern on both academic and the industrial environments.

In the current study, the simulations have been carried out by keeping excess air ratio, fuel and air inlet cross-sectional areas, area of the outlet and ideal heat outputs of the system (thus, different mass flow rates for each gas) as constants. Therefore, it was possible to observe only the effects of the geometric adjustments and the fuel compositions. In addition, a comparison between a linear eddy viscosity turbulence model and a non-linear eddy viscosity model has been given in the manuscript.

Results showed that significant amount of improvement was achieved due to the changes in the geometry. Temperature difference that was evaluated is around 200 - 300 degrees at the outlet boundary. The preheating effect as it can be understood from the results, increase combustion efficiency (providing the necessary amount of energy to heat the mixture to react). And at the same time, the heat loss in the case of conventional design was regained by the heat transfer between the flue gas and the combustion air with the preheating design concept. Therefore, significant amount of energy has been saved.

On the other hand, FGR also increased the combustion efficiency, which led to lower

emissions. Flue gas recirculation has provided the best possible option on its own in terms of all types of emission discharge. However, there can be other and also coupled systems which may be way more effective in supplying both thermally efficient and less pollutant designs at the same time. Compared to the rest of the designs including the conventional burner, Burner – 1 appeared to be the best choice among the others which has a dominant IFGR effect coupled with preheating.

Also, it could be said that k- $\epsilon$  turbulence model is suitable enough to model such a system at a certain level of accuracy compared to a non-linear model. However, the differences are not negligible considering the emission levels that have been evaluated in the current study. Since, the performances of different designs can be evaluated wrongly.

For the future study, a parametric study coupled with an optimization code will be carried out using all these concepts and more to reveal the best design and operating conditions. With the state-of-the-art technologies on burner and furnace designs and integrating them together in an optimized design, above values can be improved even further which will result in a sustainable and better future for next generations.

## REFERENCES

- Albrecht, F. G., D. H. König, N. Baucks and R.-U. Dietrich (2017). A standardized methodology for the techno-economic evaluation of alternative fuels – A case study. *Fuel* 194, 511–526.
- ANSYS. (2017). *ANSYS Fluent Theory Guide 17.2* (17.2). Canonsburg, PA.
- Cappelletti, A., and F. Martelli (2017). Investigation of a pure hydrogen fueled gas turbine burner. *International Journal of Hydrogen Energy* 42(15), 10513–10523.
- Chen, S., Y. Xing and A. Li (2017). CFD investigation on Low-NO<sub>x</sub> strategy of folded flame pattern based on fuel-staging natural gas burner. *Applied Thermal Engineering* 112(5), 1487–1496.
- Colannino, J. (2006). *Modeling of combustion systems : a practical approach*. CRC/Taylor & Francis, Florida, USA.
- Craft, T. J., B. E. Launder and K. Suga (1996). Development and application of cubic eddy viscosity model of turbulence. *International Journal of Heat and Fluid Flow* 17, 108–115.
- Förster, T., Y. Voloshchuk, A. Richter and B. Meyer (2017). 3D numerical study of the performance of different burner concepts for the high-pressure non-catalytic natural gas reforming based on the Freiberg semi-industrial test facility HP POX. *Fuel* 203, 954–963.
- Frouzakis, C. E. (2011). *Lattice Boltzmann Methods for Reactive and Other Flows*. Springer Netherlands. Turbulent Combustion Modeling.
- Gaikwad, P., H. Kulkarni and S. Sreedhara (2017). Simplified numerical modelling of oxy-fuel combustion of pulverized coal in a swirl burner. *Applied Thermal Engineering* 124, 734–745.
- Hanjalić, K., and B. Launder (2011). *Modelling turbulence in engineering and the environment: second-moment routes to closure*. Cambridge University Press, Cambridge, UK..
- Harish, A., H. R. Rakesh Ranga, A. Babu and V. Raghavan (2018). Experimental study of flame characteristics and stability regimes of biogas – Air cross flow non-premixed flames. *Fuel* 223, 334–343.
- Haworth, D. C. (2010). Progress in probability density function methods for turbulent reacting flows. *Progress in Energy and Combustion Science* 36(2), 168–259.
- İlbaş, M., M. Şahin and S. Karyeyen (2018). 3D numerical modelling of turbulent biogas combustion in a newly generated 10 KW burner. *Journal of the Energy Institute* 91(1), 87–99.
- Chacón, J., J. M. Sala and, J. M. Blanco (2007). Investigation on the Design and Optimization of a Low NO<sub>x</sub>-CO Emission Burner Both Experimentally and through Computational Fluid Dynamics (CFD) Simulations. *Energy & Fuels* 21(1), 42–58.
- Jerzak, W. (2018). Extinction limits of swirl non-premixed methane flames and CH<sub>4</sub>/C<sub>x</sub>H<sub>y</sub>/N<sub>2</sub> mixtures: experimental evaluation and thermodynamic calculations. *Energy & Fuels* 32(6), 7179–7187.
- Jovanović, R. D., K. Strug, B. Swiatkowski, S. Kakietek, K. Jagiello and D. B. Cvetinović (2017). Experimental and numerical investigation of flame characteristics during swirl burner operation under conventional and oxy-fuel conditions. *Thermal Science* 21(3), 1463–1477.
- Baukal Jr., C. E. (2013). *The John Zink Hamworthy Combustion Handbook, Second Edition: Volume 2 – Design and Operations*. CRC Press, Taylor & Francis Group, Florida, USA.
- Kakaç, S., A. Pramuanjaroenkij and X. Y. Zhou (2007). A review of numerical modeling of solid oxide fuel cells. *International Journal of Hydrogen Energy* 32(7), 761–786.
- Kuang, M., Z. Li, Z. Ling and X. Zeng (2014). Improving flow and combustion performance of a large-scale down-fired furnace by shortening secondary-air port area. *Fuel* 121, 232–239.
- Launder, B. E., Reece, G. J. and Rodi W. (1975). Progress in the development of a reynolds-stress turbulence closure. *Journal of Fluid Mechanics* 68(3), 537–566.

- Liu, B., B. Bao, Y. Wang and H. Xu (2017). Numerical simulation of flow, combustion and NO emission of a fuel-staged industrial gas burner. *Journal of the Energy Institute* 90(3), 441–451.
- Mohammed, A. N., E. V. Jithin, L. Dineshkumar, V. Ratna Kishore and A. Mohammad (2018). Tip Opening of Burner-Stabilized Flames. *Energy & Fuels* 32(2), 2344–2354.
- Ouali, S., A. H. Bentebbiche and T. Belmrabet (2016). Numerical simulation of swirl and methane equivalence ratio effects on premixed turbulent flames and NOx apparitions. *Journal of Applied Fluid Mechanics* 9(2), 987–998.
- Pedersen, M. N., M. Nielsen, S. Clausen, P. A. Jensen, L. Skaarup Jensen and K. Dam-Johansen (2017). Imaging of Flames in Cement Kilns To Study the Influence of Different Fuel Types. *Energy & Fuels* 31(10), 11424–11438.
- Perpignan, A. A. V., M. G. Talboom, Y. Levy and A. G. Rao (2018). Emission Modeling of an Interturbine Burner Based on Flameless Combustion. *Energy & Fuels* 32(1), 822–838.
- Rashwan, S. S. (2018). The Effect of Swirl Number and Oxidizer Composition on Combustion Characteristics of Non-Premixed Methane Flames. *Energy & Fuels* 32(2), 2517–2526.
- Shih, T.-H., W. W. Liou, A. Shabbir, Z. Yang and J. Zhu (1995). A new  $k-\epsilon$  eddy viscosity model for high reynolds number turbulent flows. *Computers & Fluids* 24(3), 227–238.
- Tannehill, J., D. A. Anderson and R. H. Pletcher (2013). *Computational Fluid Mechanics and Heat Transfer*. CRC Press, Taylor & Francis Group, Florida, USA..
- Tu, Y., A. Zhou, M. Xu, W. Yang, K. B. Siah and P. Subbaiah (2018). NOX reduction in a 40 t/h biomass fired grate boiler using internal flue gas recirculation technology. *Applied Energy* 220, 962–973.
- Turns, S. R. (2012). *An introduction to combustion : concepts and applications*. McGraw-Hill, New York, USA..
- Vega, F., F. Benjumea, B. Navarrete and E. Portillo (2015). Geometrical parameter evaluation of a 0.5 MWth bench-scale oxy-combustion burner. *Fuel* 139, 637–645.
- Zhang, T. H., F. G. Liu and X. Y. You (2014). Optimization of gas mixing system of premixed burner based on CFD analysis. *Energy Conversion and Management* 85, 131–139.
- Zhen, H. S., J. Miao, C. W. Leung, C. S. Cheung and Z. H. Huang (2016). A study on the effects of air preheat on the combustion and heat transfer characteristics of Bunsen flames. *Fuel* 184, 50–58.
- Zhou, H., Y. Yang, H. Liu and Q. Hang (2014). Numerical simulation of the combustion characteristics of a low NOx swirl burner: Influence of the primary air pipe. *Fuel* 130, 168–176.